Title
Direct mapping of curve-crossing dynamics in IBr by attosecond transient absorption spectroscopy

Journal
Science, 365(6448)

ISSN
0036-8075

Authors
Kobayashi, Yuki
Chang, Kristina F
Zeng, Tao
et al.

Publication Date
2019-07-05

DOI
10.1126/science.aax0076

Peer reviewed

CHEMICAL PHYSICS

Direct mapping of curve-crossing dynamics in IBr by attosecond transient absorption spectroscopy

Yuki Kobayashi[1]*, Kristina F. Chang[1], Tao Zeng[2], Daniel M. Neumark[1,3]*, Stephen R. Leone[1,3,4]*

The electronic character of photoexcited molecules can abruptly change at avoided crossings and conical intersections. Here, we report direct mapping of the coupled interplay between electrons and nuclei in a prototype molecule, iodine monobromide (IBr), by using attosecond transient absorption spectroscopy. A few-femtosecond visible pulse resonantly excites the ($B^3\Pi_{0^+}$), Y(0^+), and Z(0^+) states of IBr, and the photodissociation dynamics are tracked with an attosecond extreme-ultraviolet pulse that simultaneously probes the I-4*d* and Br-3*d* core-level absorption edges. Direct comparison with quantum mechanical simulations unambiguously identifies the absorption features associated with adiabatic and diabatic channels at the B/Y avoided crossing and concurrent two-photon dissociation processes that involve the Y/Z avoided crossing. The results show clear evidence for rapid switching of valence-electronic character at the avoided crossing.

The conventional picture of a photoexcited molecule smoothly evolving toward a product state on a single potential surface is invalid when degeneracies between neighboring states induce nonadiabatic interactions (*1*–*3*). Molecular dynamics that involve avoided crossings and conical intersections have been of fundamental interest in chemical physics since the seminal Landau-Zener model pioneered in the 1930s (*4*, *5*). It is now widely accepted that nonadiabatic interactions play key roles in broad classes of photochemical reactions, such as photoisomerization in the retinal chromophore (*6*) and photostability of DNA base pairs against ultraviolet radiation (*7*). Realization of laser-based control of nonadiabatic processes represents a pivotal milestone in recent progress of molecular spectroscopy (*8*, *9*).

Despite these successes, real-time observation of electronic dynamics in nonadiabatic regions remains elusive (*10*). Conceptually, electronic character can rapidly change in synchrony with nuclear motion. Experimentally, few-femtosecond time resolution is required for the probe, and the intrinsic degeneracy makes it challenging to obtain state-resolved information. Several experimental methods have been applied to this end (*11*–*15*), including high-harmonic spectroscopy (*16*) and ultrafast electron diffraction (*17*). Recent theoretical studies predicted that transient absorption spectroscopy in the x-ray/extreme-ultraviolet (XUV) range offers a distinct and powerful route to measure excited-state dynamics around nonadiabatic regions, with core-level absorption capturing the marked reorganization of valence electrons (*18*, *19*). Core-level absorption has superb state resolution (*20*); not only spin-orbit fine structure but even near-degenerate electronic states in nonadiabatic regions can be clearly resolved, as we demonstrate in this work. The probe step of core-to-valence transitions, being free of strong-field processes, can be directly simulated with quantum-chemistry calculations (*21*). Furthermore, when combined with high-harmonic generation–based attosecond light sources, this all-optical method has the potential to attain subfemtosecond probing time resolution (*22*).

Here, we report attosecond transient absorption mapping of valence-electron dynamics accompanying visible-light excitation of iodine monobromide (IBr), a prototype molecule for nonadiabatic photodissociation dynamics (*23*, *24*). Our primary focus is the switching of electronic character ensuing at an avoided crossing between excited $B(^3\Pi_{0^+})$ and Y(0^+) states. An outline of the experiment is depicted in Fig. 1A. Photodissociation is triggered by a few-femtosecond visible pump pulse [wavelength (λ) = 530 nm, $\Delta\lambda$ = 70 nm, 8 fs, 15 μJ] (Fig. 1B), which selectively excites the visible absorption band of IBr (Fig. 1B) (*25*) and minimizes the unfavorable ionization effects that arise in more conventional experiments in which intense near-infrared excitation is used (*26*). In the probe step after a delay time τ, an attosecond XUV pulse produced through high-harmonic generation is introduced (45 to 72 eV, ~200 as) (Fig. 1C), which encodes the time evolution of the photoexcited molecule in the characteristic core-to-valence absorption signals. The XUV probe pulse simultaneously detects the two core-level absorption edges of IBr: the $N_{4,5}$ edge (4*d* orbitals) of iodine and the $M_{4,5}$ edge (3*d* orbitals) of bromine. This feature enables full tracking of both photofragment electronic states, providing considerably more insight than experiments in which only one fragment is tracked (*15*).

The potential energy curves of IBr are shown in Fig. 1D. Multiple avoided crossings are present in diatomic interhalogens because of the strong spin-orbit couplings of the halogen atoms and the absence of *g*-*u* symmetry for heteronuclear diatomics (*23*, *24*). Two physical pictures are invoked to describe the dynamics at avoided crossings (*27*); in a diabatic picture, electronic states conserve their character as they move along the reaction coordinate, whereas in an adiabatic picture, electronic states are eigenstates of the electronic Hamiltonian and are subject to switching of electronic character. The visible pump pulse excites the molecule to an attractive $B(^3\Pi_{0^+})$ state, which undergoes an avoided crossing with a repulsive Y(0^+) state [distance of crossing (R_c) = 3.3 Å]. In the diabatic channel at the B/Y avoided crossing (Fig. 1D, inset), the photoexcited molecule remains on the attractive $B(^3\Pi_{0^+})$ potential, conserving its electronic character, and evolves toward the spin-orbit excited $I(^2P_{3/2}) + Br^*(^2P_{1/2})$ asymptote. In the adiabatic channel (Fig. 1D, inset), the photoexcited molecule transfers to the repulsive Y(0^+) potential, rapidly switching its electronic character, and proceeds to the ground $I(^2P_{3/2}) + Br(^2P_{3/2})$ asymptote. The nonadiabatic coupling is of intermediate strength for the B/Y avoided crossing of IBr, and the measured dissociation ratio between the diabatic and adiabatic channels is approximately 3:1 (*28*). In the experiments, resonance-enhanced two-photon processes are also observed for the visible pump pulse, which reaches a peak-field intensity of ~5×10^{13} W/cm^2. An electronic-structure analysis reveals a large transition dipole moment (~3 D) associated with the B → Y transition (*26*). The Y(0^+) state undergoes an avoided crossing with the higher Z(0^+) state (R_c = 2.8 Å), and the dissociation across the Y/Z avoided crossing leads to the $I^*(^2P_{1/2}) + Br(^2P_{3/2})$ asymptote. The B → Z transition is also possible but of less importance (~20% compared with B → Y) and is not considered further here.

We first analyzed the transient absorption spectrum of the dissociation products (Fig. 2A, recorded at delay times from 215 to 245 fs). The differential optical density (ΔOD) is defined as a logarithmic ratio of the transmitted XUV spectra with and without the visible pump pulse. Iodine and bromine atoms each exhibit three absorption lines in the I 4*d* → 5*p* and Br 3*d* → 4*p* series: 45.9, 46.7, and 47.6 eV for I and 64.5, 65.1, and 65.6 eV for Br, corresponding to the $^2P_{3/2} \rightarrow {}^2D_{5/2}$, $^2P_{1/2} \rightarrow {}^2D_{3/2}$, and $^2P_{3/2} \rightarrow {}^2D_{3/2}$ transitions, respectively (*29*, *30*). In Fig. 2A, the product ratio between the Br and Br* atoms calculated from the XUV absorption amplitudes is Br*/Br = 3.3, which is in reasonable agreement with a previous measurement at 525-nm excitation (Br*/Br = 3.0) (*28*). At the same time, a sizable signal from the I* atom is observed, yielding a product ratio of I*/I = 0.5. The appearance energy of the I* atom (~2.8 eV) is higher than the center photon energy of the visible pump pulse (~2.3 eV); thus, this signal is attributed to two-photon (or

[1]Department of Chemistry, University of California, Berkeley, CA 94720, USA. [2]Department of Chemistry, Carleton University, Ottawa, Ontario K1S5B6, Canada. [3]Chemical Sciences Division, Lawrence Berkeley National Laboratory, Berkeley, CA 94720, USA. [4]Department of Physics, University of California, Berkeley, CA 94720, USA.
*Corresponding author. Email: ykoba@berkeley.edu (Y.K.); dneumark@berkeley.edu (D.M.N.); srl@berkeley.edu (S.R.L.)

multiphoton) visible-excitation processes. A group of weak absorption signals at 55 to 58 eV corresponds to the I $4d \rightarrow np$ ($n > 5$) Rydberg series (*31*).

Transient absorption spectra as a function of delay time are shown in Fig. 2B. The measurements are carried out from −16 to 245 fs delay time at 1.5-fs intervals. To calculate ΔOD, the pump-on/pump-off XUV spectra were each averaged over 200 frames (40 laser pulses per frame). In Fig. 2B, the excited-state absorption (ΔOD > 0) is shown in bright colors, and the ground-state bleach (ΔOD < 0) is shown in gray shades. The observed ground-state bleach features, both in the I-4*d* and Br-3*d* windows, exhibit signatures of vibrational coherences in the ground $X(^1\Sigma_{0^+})$ state [isotopic averages: vibrational frequency (ω_e) = 268 m^{-1}, anharmonicity ($\omega_e x_e$) = 0.8 cm^{-1}, vibrational period (T) = 125 fs] (*32*). In previous studies, vibrational coherences in the neutral ground states launched by strong-field ionization were reported (*33*, *34*). In this work, the excitation mechanism is a resonant single-photon process, and distinct nodal structures are observed in the oscillating absorption signals. We performed quantum wave-packet simulations to compute the core-level absorption spectra, and the observed features are reproduced by taking coherences in the v = 0, 1, and 2 vibrational states (fig. S3). The mechanism for the overtone (v = 2) excitation is attributed to a stimulated Raman process enhanced by resonant visible-light coupling between the $X(^1\Sigma_{0^+})$ and $B(^3\Pi_{0^+})$ states.

The details of the excited-state absorption in the I-4*d* and Br-3*d* windows are shown in Fig. 3, A and B, respectively. The early time signals (0 to 50 fs) exhibit sweeping shifts to lower photon energy, which is indicative of molecular dissociation proceeding on the $B(^3\Pi_{0^+})$ potential. The evolution of the photoexcited molecule at the B/Y avoided crossing is encoded in the subsequent temporal window (50 to 80 fs) (Fig. 3, A and B, dashed boxes), and the corresponding absorption traces taken at 6-fs intervals are shown in Fig. 3, C and D (50, 56, 62, 68, 74, and 80 fs). The sharp absorption features associated with the I*(46.7 eV) and Br*(65.1 eV) atoms are nearly invariant with respect to delay time. These atomic fragments conceivably originate from two-photon processes that occur on a shorter time scale, an assignment that was corroborated with ab initio simulations. The other broad signals (indicated in Fig. 3 with arrows labeled "diabatic" and "adiabatic") exhibit dramatic variations both in the absorption amplitude and energy. As already mentioned, the diabatic channel at the B/Y avoided crossing leads to the I + Br* asymptote (Fig. 1D), and the associated wave packet conserves its electronic character. In the experimental results of the Br-3*d* window (Fig. 3D), the absorption signal that exhibits continuous shifts to lower photon energy converges to the Br* absorption line and hence is assigned to the diabatic channel. In the adiabatic channel, however, the photoexcited molecule changes the electronic character and proceeds to the ground I + Br

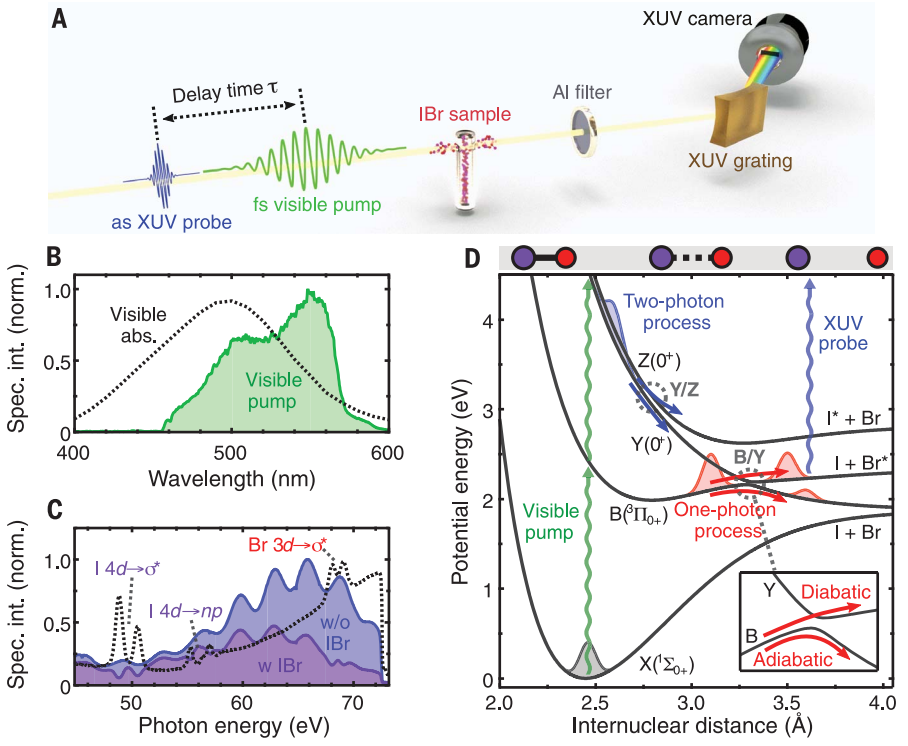

Fig. 1. Outline of experiment. (**A**) Illustration of the experimental setup. (**B**) Spectral intensity of the visible pump pulse (green area) and visible-absorption band (extinction coefficient) of IBr (black dashed curve) measured previously in (*25*). (**C**) Spectral intensity of the XUV probe pulse recorded with (purple area) and without (blue area) the IBr sample and the optical density (black dashed curve) calculated from the two spectra. The I-4*d* and Br-3*d* edges are covered by the broadband XUV spectrum. (**D**) Adiabatic potential energy curves of IBr, with the visible and XUV excitation pathways indicated with vertical arrows. The red and blue wave packets indicate the dissociation pathways from one-photon and two-photon processes, respectively. Avoided crossings are formed between the B and Y states (R_c = 3.3 Å) and Z and Y states (R_c = 2.8 Å). (Inset) The adiabatic and diabatic channels at the B/Y avoided crossing.

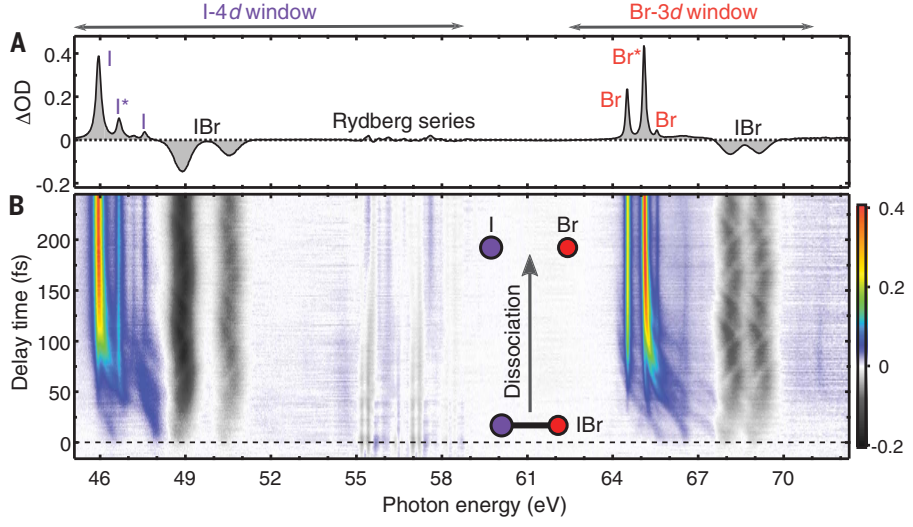

Fig. 2. Core-level transient absorption spectra of IBr. (**A**) Transient absorption spectrum of the dissociation products recorded at delay times from 215 to 245 fs. (**B**) Delay-time-resolved transient absorption spectra. At zero delay time, the visible pump pulse initiates the dissociation processes, and excited-state signal (bright colors) as well as ground-state bleach (gray shades) emerge. The dissociation proceeds toward the positive delays.

asymptote (Fig. 1D). In the experimental results (Fig. 3D), the Br absorption line suddenly emerges accompanied by no energy shift at a separate photon energy. The discontinuous evolution of the Br signal is a manifestation of the new electronic character acquired from the neighboring $Y(0^+)$ state. In the I-4*d* window (Fig. 3C), the XUV absorption signals associated with the diabatic and adiabatic channels are not as widely separated as in the Br-3*d* window because the same I atom is produced in both channels. Nonetheless, the continuous shifts to lower photon energy and the sudden emergence of the sharp I signal are distinctly resolved, leading to consistent assignments of the B/Y avoided-crossing signals.

To gain more detailed insight into the transitory molecular features, we performed ab initio simulations of the core-level absorption spectra (*26*). The valence and core-excited electronic structures were computed by means of spin-orbit generalized multiconfigurational quasi-degenerate perturbation theory (SO-GMC-QDPT) (*21*, *35*), and from these, the XUV absorption strengths were obtained. Nonadiabatic dissociation dynamics were simulated fully quantum mechanically by numerically solving the time-dependent Schrödinger equation. The initial wave packets were taken to be in the Franck-Condon region of the $B(^3\Pi_{0^+})$ state (one-photon process) or on the $Y(0^+)$ state (two-photon process) to model the relevant visible-light excitations.

Simulated results for the one-photon process are shown in Fig. 3, E and F. The sweeping energy shifts in the early time window are successfully reproduced by the simulation. The $B(^3\Pi_{0^+})$ state in the Franck-Condon region has a $[\sigma^2\pi^4\pi^{*3}\sigma^{*1}]$ configuration and is probed by the core-level transitions to the π^* and σ^* orbitals. The observed absorption lines reflect the multiplet structures of the core-excited states that originate from the spin-orbit couplings in the core (I-4*d*, Br-3*d*) and valence (π, π^*) orbitals (fig. S6). Some features are broadened and less pronounced in the experiments compared with the simulations, which we attribute to the finite spectral width of the visible pump pulse and the nuclear wave-packet motion on the repulsive core-excited potentials. The absorption traces in the temporal window for the B/Y avoided crossing (50 to 80 fs) are shown in Fig. 3, G and H, with assignments of the diabatic and adiabatic channels directly made from the wave-packet simulations. The continuous (diabatic) and discontinuous (adiabatic) evolution of the XUV absorption signals exhibits an excellent match with the experiments, providing clear confirmation of the experimental signal assignments at the B/Y avoided crossing.

The origin of the I* and part of the Br* signals is verified with the two-photon simulations (Fig. 3, I and J). The simulated I* signal (Fig. 3I) matches the experimental result (Fig. 3A) both in time and absorption energy. Passage through the Y/Z avoided crossing (Fig. 1D) is calculated to occur in ~25 fs. These early time dynamics are not as clearly resolved in the experiments because of the spectral broadening from the fast dissociative motion in the two-photon processes. Calculated absorption strengths of the $Y(0^+)$ and $Z(0^+)$ states are provided in fig. S7 for future reference. The Br* atom is produced by way of the wave packet adiabatically transferring from the repulsive $Y(0^+)$ potential to the attractive $B(^3\Pi_{0^+})$ potential at the B/Y avoided crossing. As such, in the simulation, the switching of electronic character causes abrupt emergence of the Br*

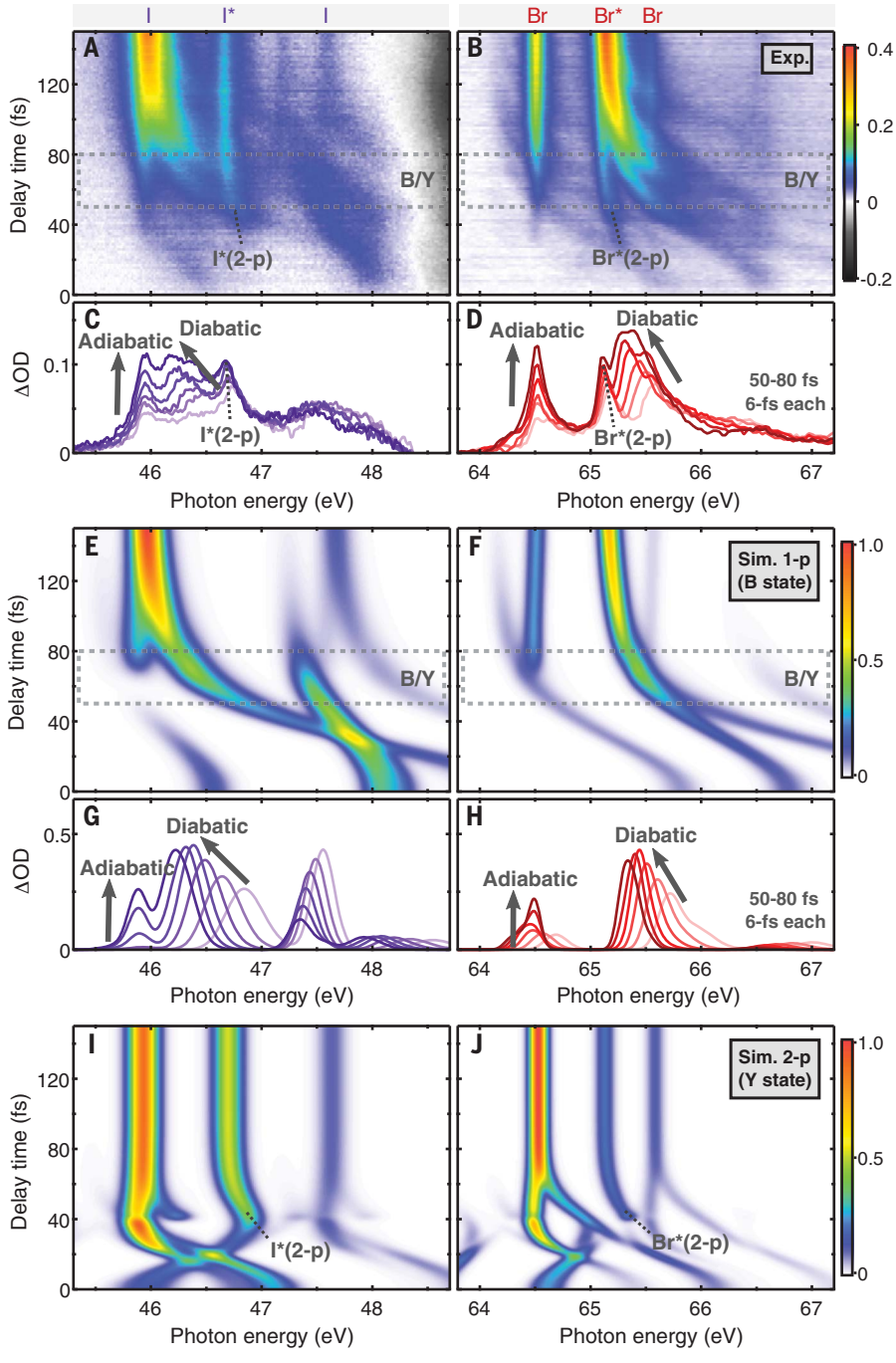

Fig. 3. Experimental and simulated spectra of nonadiabatic dissociation dynamics. (**A** and **B**) Experimental absorption spectra in the (A) I-4*d* and (B) Br-3*d* windows, respectively. The temporal window for the B/Y avoided crossing is highlighted with dashed boxes. (**C** and **D**) Absorption spectra taken from the experimental results at delay times of 50, 56, 62, 68, 74, and 80 fs. The assignments at the adiabatic and diabatic channels at the B/Y avoided crossing are denoted. (**E** to **H**) One-photon (1-p) simulation results shown for the comparison with the experimental results (A) to (D). (**I** and **J**) Two-photon (2-p) simulation results that reproduce the early time emergences of the I* and Br* signals. The absorption signals in the one-photon and two-photon simulations are normalized independently.

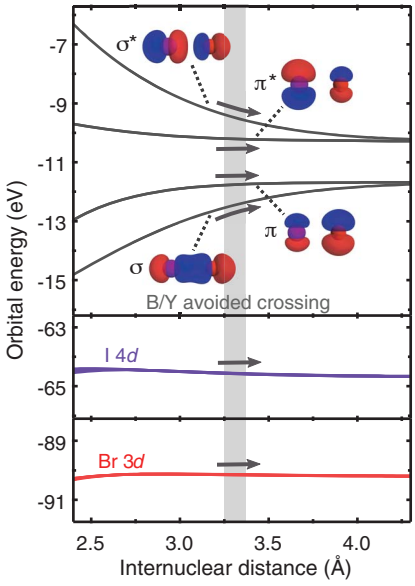

Fig. 4. Orbital energies as a function of internuclear distance. The energy difference between the core and valence orbitals are closely tied to the observed absorption energies. Around the B/Y avoided crossing (gray area), the energies of the core orbitals and valence π/π^* orbitals are nearly invariant, whereas those of the σ/σ^* orbitals show increase or decrease versus internuclear distance. The displayed molecular orbitals are computed at R_c = 3.3 Å.

signal (Fig. 3J), and the corresponding absorption feature is resolved at ~40-fs delay time in the experimental results (Fig. 3B).

To further investigate the electronic-structure information at the B/Y avoided crossing imprinted in the core-level absorption spectra, we examined the orbital energies and electron configurations. The energies of the active molecular orbitals are shown in Fig. 4 as a function of internuclear distance computed at the level of multiconfigurational self-consistent field (MCSCF). The energy differences between the core and valence orbitals are closely tied to the observed absorption energies. The exact description of the electronic states requires multiconfigurational treatments and inclusion of spin-orbit couplings, as is done in the SO-GMC-QDPT calculations (*26*). The energies of the I-4*d* and Br-3*d* orbitals are nearly invariant throughout the reaction coordinate. This insensitivity to internuclear distance indicates that the observed energy shifts in the diabatic channel (or no shift in the adiabatic channel) reflect the energy variations in the valence orbitals alone. As for the valence orbitals, the energy gradients quantified at the B/Y avoided crossing (gray area) are +1.5 eV/Å and −1.7 eV/Å for σ and σ*, respectively, but only +0.3 eV/Å and −0.2 eV/Å for π and π*, respectively. These trends indicate that the π and π* orbitals are effectively no longer contributing to the variation of the potential energies when the wave packet reaches the avoided crossing. A more direct clue to the electronic-character switching is obtained from the electronic configurations computed for each adiabatic state (*36*–*38*). Just before the avoided crossing, the $B(^3\Pi_{0^+})$ state is a mixed configuration of $[\sigma^2\pi^4\pi^{*3}\sigma^{*1}]$ and $[\sigma^2\pi^3\pi^{*4}\sigma^{*1}]$; a single vacancy lies in σ*, and the other vacancy is distributed between π and π*. After the photoexcited molecule adiabatically transfers to the repulsive $Y(0^+)$ potential, the main configuration changes to $[\sigma^2\pi^3\pi^{*3}\sigma^{*2}]$, where the σ* orbital is fully occupied, and the two vacancies lie in the π and π* orbitals. A physical picture emerges from these results: The vacancy in the valence orbitals switches from σ* to π/π* at the B/Y avoided crossing, giving rise to new core-level absorption signals with no further energy shifts, reflecting the energy invariance of the π and π* orbitals versus internuclear distance.

The visible-absorption band of IBr is a key benchmark system for curve-crossing dynamics. We applied attosecond transient absorption spectroscopy in combination with the SO-GMC-QDPT calculations of the electronic structures and revealed the switching of the valence-orbital vacancy from σ* to π/π* at the B/Y avoided crossing. This intuitive picture was obtained by the powerful ability of the attosecond XUV pulse to sensitively encode the energies and occupancies of valence orbitals in the core-to-valence absorption spectra of IBr. The valence-electronic structure not only determines the strength of chemical bonds, it also governs the reactivity of a molecule as represented by frontier-orbital theory; unraveling the dramatic evolution of valence-electronic structures around nonadiabatic regions will greatly extend knowledge of photochemical reactions. Application of ultrafast x-ray/XUV light sources in the explorations of chemical dynamics is an actively advancing field of research (*39*, *40*), and this work shows the great promise of attosecond transient absorption spectroscopy for mapping the evolution of valence electrons in larger molecular systems.

REFERENCES AND NOTES

1. G. A. Worth, L. S. Cederbaum, *Annu. Rev. Phys. Chem.* **55**, 127–158 (2004).
2. B. G. Levine, T. J. Martínez, *Annu. Rev. Phys. Chem.* **58**, 613–634 (2007).
3. M. P. Bircher *et al.*, *Struct. Dyn.* **4**, 061510 (2018).
4. L. D. Landau, *Phys. Z. Sowjetunion* **2**, 46 (1932).
5. C. Zener, R. H. Fowler, *R. Soc. London Ser. A* **137**, 696–702 (1932).
6. D. Polli *et al.*, *Nature* **467**, 440–443 (2010).
7. T. Schultz *et al.*, *Science* **306**, 1765–1768 (2004).
8. B. J. Sussman, D. Townsend, M. Y. Ivanov, A. Stolow, *Science* **314**, 278–281 (2006).
9. M. E. Corrales *et al.*, *Nat. Chem.* **6**, 785–790 (2014).
10. S. R. Leone *et al.*, *Nat. Photonics* **8**, 162–166 (2014).
11. S. Takeuchi *et al.*, *Science* **322**, 1073–1077 (2008).
12. M. C. E. Galbraith *et al.*, *Nat. Commun.* **8**, 1018 (2017).
13. A. von Conta *et al.*, *Nat. Commun.* **9**, 3162 (2018).
14. A. E. Boguslavskiy *et al.*, *J. Chem. Phys.* **148**, 164302 (2018).
15. H. Timmers *et al.*, *Nat. Commun.* 10.1038/s41467-019-10789-7 (2019).
16. H. J. Wörner *et al.*, *Science* **334**, 208–212 (2011).
17. J. Yang *et al.*, *Science* **361**, 64–67 (2018).
18. S. P. Neville *et al.*, *Faraday Discuss.* **194**, 117–145 (2016).
19. S. P. Neville, M. Chergui, A. Stolow, M. S. Schuurman, *Phys. Rev. Lett.* **120**, 243001 (2018).
20. R. Geneaux, H. J. B. Marroux, A. Guggenmos, D. M. Neumark, S. R. Leone, *Philos. Trans. A Phys. Eng. Sci.* **377**, 20170463 (2019).
21. Y. Kobayashi, T. Zeng, D. M. Neumark, S. R. Leone, *Struct. Dyn.* **6**, 014101 (2019).
22. F. Krausz, M. Ivanov, *Rev. Mod. Phys.* **81**, 163–234 (2009).
23. M. S. Child, R. B. Bernstein, *J. Chem. Phys.* **59**, 5916–5925 (1973).
24. M. S. Child, *Mol. Phys.* **32**, 1495–1510 (1976).
25. D. J. Seery, D. Britton, *J. Phys. Chem.* **68**, 2263–2266 (1964).
26. Materials and methods are available as supplementary materials.
27. T. Van Voorhis *et al.*, *Annu. Rev. Phys. Chem.* **61**, 149–170 (2010).
28. E. Wrede *et al.*, *J. Chem. Phys.* **114**, 2629–2646 (2001).
29. L. Nahon, P. Morin, F. C. Farnoux, *Phys. Scr.* **T41**, 104–112 (1992).
30. G. O'Sullivan, C. McGuinness, J. T. Costello, E. T. Kennedy, B. Weinmann, *Phys. Rev. A* **53**, 3211–3226 (1996).
31. L. Nahon, P. Morin, *Phys. Rev. A* **45**, 2887–2893 (1992).
32. R. E. Willis Jr., W. W. Clark III, *J. Chem. Phys.* **72**, 4946–4950 (1980).
33. E. R. Hosler, S. R. Leone, *Phys. Rev. A* **88**, 023420 (2013).
34. Z. Wei *et al.*, *Nat. Commun.* **8**, 735 (2017).
35. T. Zeng, *J. Chem. Phys.* **146**, 144103 (2017).
36. S. Patchkovskii, *Phys. Chem. Chem. Phys.* **8**, 926–940 (2006).
37. R. Li *et al.*, *J. Quant. Spectrosc. Radiat. Transf.* **133**, 271–280 (2014).
38. T. Matsuoka, S. Yabushita, *J. Phys. Chem. A* **119**, 9609–9620 (2015).
39. M. Chergui, A. H. Zewail, *ChemPhysChem* **10**, 28–43 (2009).
40. P. M. Kraus, M. Zürch, S. K. Cushing, D. M. Neumark, S. R. Leone, *Nat. Rev. Chem.* **2**, 82–94 (2018).
41. Y. Kobayashi, K. Chang, T. Zeng, D. Neumark, S. Leone, Direct mapping of curve crossing dynamics in IBr by attosecond transient absorption spectroscopy, UC Berkeley Dash, Dataset (2019); doi:10.6078/D10X1Z.

ACKNOWLEDGMENTS

Funding: This work, Y.K., and K.F.C. were supported by the National Science Foundation (NSF) (CHE-1660417). Y.K., K.F.C., D.M.N., and S.R.L. also acknowledge the funding from the U.S. Army Research Office (ARO) (W911NF-14-1-0383). T.Z. acknowledges the Natural Sciences and Engineering Research Council (NSERC) of Canada for research funding (RGPIN-2016-06276) and also Carleton University for the start-up grant (186853). Some of the computations by Y.K. were performed by using workstations at the Molecular Graphics and Computation Facility (MGCF) at the University of California, Berkeley, which is supported by the National Institutes of Health (NIH) (S10OD023532). Y.K. also acknowledges financial support from the Funai Overseas Scholarship.
Author contributions: Y.K., D.M.N., and S.R.L. conceived the experiments. Y.K. and K.F.C. performed the attosecond transient absorption measurements. T.Z. developed the SO-GMC-QDPT code. Y.K. performed the electronic-structure calculations and quantum-mechanical simulations. Y.K. analyzed the results and wrote the manuscript, with inputs from all authors.
Competing interests: The authors declare no competing interests. **Data and materials availability:** The experimental results of the attosecond transient absorption measurements are archived in the Dash repository (*41*).

SUPPLEMENTARY MATERIALS

science.sciencemag.org/content/365/6448/79/suppl/DC1
Materials and Methods
Supplementary Text
Figs. S1 to S8
Tables S1 and S2
References (*42*–*60*)

5 March 2019; accepted 11 June 2019
10.1126/science.aax0076

Direct mapping of curve-crossing dynamics in IBr by attosecond transient absorption spectroscopy

Yuki Kobayashi, Kristina F. Chang, Tao Zeng, Daniel M. Neumark and Stephen R. Leone

Science **365** (6448), 79-83.
DOI: 10.1126/science.aax0076

A panoramic view of photodissociation

As light pulses get shorter in time, they correspondingly get broader in frequency. Kobayashi *et al.* take advantage of both properties of attosecond pulses to elucidate iodine monobromide (IBr) photodissociation by detecting ultrafast b romine and iodine spectral shifts simultaneously. A preliminary burst of light weakens the I–Br bond. Then, as the atoms fly apart, they reach a configuration where the bond vibration can couple ground and excited electronic states. The broadband probe pulse reveals rapid changes in each atom's electronic structure at this juncture.

Science, this issue p. 79